A Single 30 cm Aperture Antenna Design for The Operation of 2 Widely Separated Frequency Bands for the Active Temperature, Ozone and Moisture Microwave Spectrometer (ATOMMS)

Sarmad. H. AlBanna, Chris Groppi, Chris Walker, Michael Schein, Steve Bell, Brian Wheelwright, Christian Drouet d'Aubigny, Abram Young, Dathon Golish, E. Robert Kursinski, Angel Otarola, Dale Ward, Kate Sammler, Willy Bertiger, Mark Miller, Herb Pickett

Abstract—***The Active Temperature Ozone and Moisture Microwave Spectrometer (ATOMMS) is an active aircraft to aircraft remote sensing occultation instrument that is designed to accurately measure the vertically resolved profiles of temperature, pressure, density, water and ozone content of the atmosphere. It uses a complimentary set of microwave transmitters and receivers in ~22 GHz and ~183 GHz water bands installed in each aircraft to measure the absorption of water and ozone as a function of altitude. Space constraints prevent the use of two separate antennas for each of these bands, so a single, dual frequency antenna system has been designed to simultaneously transmit and receive these two widely spaced frequency bands. This paper presents a detailed design of a HDPE anti-reflection grooved lens antenna that is illuminated by 2 separate, coaxially mounted feed horns for the two different frequency bands. We present the design, optimization and initial testing of the feed and lens system***.

***Index Terms*—Beam waist, Corrugated Feed Horn, Edge Taper,**

Manuscript received 26 May 2009.

Sarmad H. Albanna (Electrical Engineer & a PhD Graduate student the college of Optical Science University of Arizona Tucson AZ 85721 USA (520-626-0226; fax: 520-621-1632; e-mail: salbanna@as.arizona.edu)

C. Groppi (NSF Astronomy and Astrophysics Postdoctoral Fellow), M. Schein, B. Wheelwright and S. Bell are with Steward Observatory, University of Arizona, Tucson, AZ 85721 USA (520-626-1627; fax: 520-621-1532; e-mail: cgroppi@as.arizona.edu).

E.R. Kursinski, D. Ward, A. Otarola and K. Sammler are with the Department of Atmospheric Sciences, University of Arizona, Tucson AZ 85721.

Christian Drouet d'Aubigny Abe Young, and Dathon Golish are with TeraVision Inc, Tucson AZ.

W. Bertiger, M. Miller and H. Picket are with the NASA Jet Propulsion Laboratory, Pasadena, CA 90220 USA.

V. INTRODUCTION

The current water vapor and temperature remote sensing Earth systems do not provide accurate, complete, nor enough data sufficient to better understand and characterize our rapidly changing climate. Each present global observation system has its own measurements limitations. At the same time they all share their biased estimates of water vapor, oxygen, and O_3 distributions and densities. The current global observing system is not able to keep up with our rapidly changing climate, and its evolving climate processes.

According to the National Academy Reports [1], it is crucial to ensure the existence of a long-term more definite observing system of variables such as temperature, precipitation, humidity, pressure, clouds and turbulence. Such systems should be able to provide a 10-100 years scale of variability and change. These set of systems should also be able to break the ambiguity of wet and dry components, as is the case for the existing GPS Radio Occultation systems, via measuring of the absorption of water-vapor, reduce ionospheric sensitivity with the use of much higher frequencies, eliminate the need of using boundary conditions and weighting factors of middle atmosphere climatology, and profile other constituents such as O_3 via absorption. Reference [2] covers in details the global measuring systems that are operating today and their limitations. The ATOMMS instrument remote sensor will bring unique new capabilities in vertical resolution, accuracy, to the global observation measurement techniques [3].

ATOMMS is an active orbiting limb-viewing spectrometer that combines the strengths of both the GPS Radio Occultation and the NASA Microwave Limb Sounder (MLS) system. With ATOMMS, the atmosphere constituent's absorbing lines are actively probed in two different microwave bands (22 GHz and 183 GHz) where there are strong water absorbing lines. With the support from NASA and NSF, and some support

from JPL, the ATOMMS group at the University of Arizona has been developing the prototype ATOMMS instrument. A prototype proof of concept instrument will be flown in specially reengineered NASA WB-57 aircraft [4]. The noses of these aircrafts have been modified such that they can carry instrumentation for weather observation in their WAVE (WB-57F Ascent Video Experiment) gimbal system. The 3 beams from the microwave transmitting and receiving bands will enter and exit the gimbal through a microwave transparent radome that will replace the front skin and optical window of the WAVE System. C. Groppi in this proceeding [5], provides a very good description of the WAVE system, the pointing operations when used for ATOMMS, a detailed description of the overall operation of the ATOMMS instrument, system architecture, electronic design and the live data recording system. Figure (2) shows one of the fully assembled ATOMMS instrument (ATOMMS A) that carries 2 microwave transmitting bands 13 GHz, and a 22 GHz band which consists of 8 fixed tones about 1 GHz wide and separated by 1 GHz spacing, as well as a receiving band at 183 GHz that includes 2 tunable tones. The second ATOMMS instrument (ATOMMS B) carries the complimentary receiver and transmitters for ATOMMS A. The 13 GHz system is a dual transmit receive system included in both instruments and is used for calibration, referencing and to provide relative phase measurement in the lower troposphere where 183 GHz signal doesn't penetrate. A detailed link budget has been developed for all the bands to simulate and or calculate the power levels at every point in the system using realistic antenna parameters and estimated losses. The specifications of all the microwave components have been derived using the link budget. Table 1 shows some of the link budget obtained parameters for the 200 GHz and 22 GHz band transmissions.

In an active sounding system such as ATOMMS, a vertical profile of the air index of refraction is obtained from the vertical profile of bending angle by means of an Abel transform [6]. The bending angle is derived from the atmospheric Doppler frequency that gets computed from the difference between the measured Doppler shift and the Doppler shift that could have been observed in the absence of the atmospheric along the signal's path.

Table 1: ATOMMS Link Budget

Symbol	Quantity description	Values
$L_{path\_200GHz\ (dB)}$ (100 km)	Free space path loss	177.5 dB for 200 GHz band 160 dB for 22 GHz band
G_{Tx}, G_{Rx}	Transmitting or Receiving antenna Gain	$G_{Rx/Tx\text{-}200GHz}$=50 dB $G_{Rx/Tx\text{-}22GHz}$=34 dB
SNR	Receiver Signal to noise ratio	$SNR_{200\ GHz}$=36.7 dB (400 KHz Bandwidth SNR_{22GHz}= 55.3 dB (50 KHz Bandwidth)

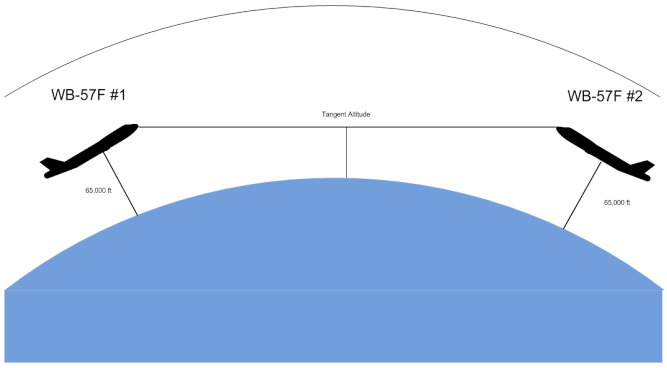

Figure 1 Aircraft to aircraft simplified occultation geometry

All the received tone's amplitudes and frequencies are derived from post processing, and by using a complete retrieval system that is under development we will be able to determine within ~100 m resolution the densities of water vapor, O_3 and the index of refraction at these higher resolution altitudes.

One of the biggest challenges of the ATOMMS prototype is antenna pointing. In order to achieve high SNR with low transmitted power, directional antennas are needed. This paper focuses on the quasi-optics subsystems and lens antenna design that plays the important role in focusing and collimating the transmitting and receiving beams.

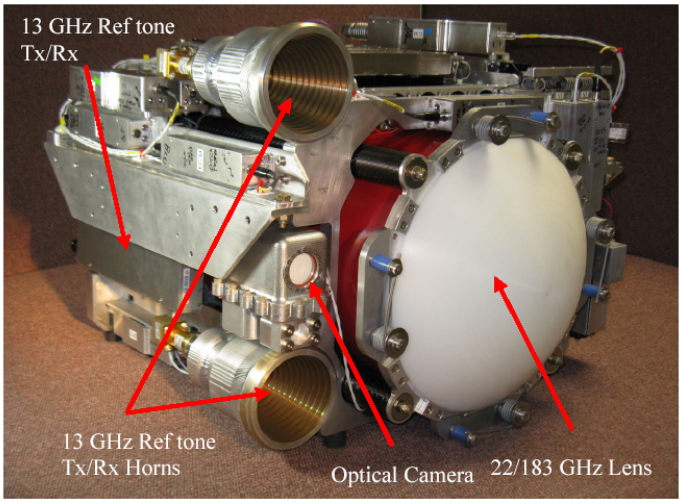

Figure 2 The ATOMMS instrument showing the 30 cm Antenna Lens and the 13 GHz TX and RX feed-horns.

VI. ATOMMS QUASIOPTICS SUBSYSTEM

The goal of the quasioptics subsystem is to produce two coaxial collimated beams using a single lens antenna. The performance was optimized for the 200 GHz such that the 22 GHz system didn't suffer from too much losses. The limited space inside the gimbal system put some constraint on the design options for the quasioptics. For example, it would have been easier to design the system such that the 22 GHz and the 200 GHz had their own separate feed and antenna, or to use reflective based antennas. In our case we employed the configuration shown in Figure (3) where the 2 feed-horns (FHs) are coaxially placed, separated by the total length of the 200 GHz FH and the polarizer that is attached to it. The FHs

are designed to symmetrically illuminate their beams into a single common refractive lens antenna. This configuration causes an obscuration of the 22 GHz beam by the 200 GHz FH and the plastic spider that holds it. The impact on the system performance will be addressed in a future section. The maximum allowed space for a lens to fit in that small geometry is about 40 cm. However, as a first step in the design, a lens of diameter D= 30 cm was chosen, since it is a standard size commonly used in the past, especially in the satellite industry. Free space Gaussian beam propagation theory has been used to analyze the beam propagation entering or existing the FHs and the lens antenna assembly. Since we illuminate the lens symmetrically, conical FHs are used with corrugations to minimize the VSWR. Corrugated conical FHs generate a balanced hybrid mode (HE11) if they are sufficiently large such that $2\pi a/\lambda > 1$, where a is the largest dimension of the source of radiation which is estimated to be 1.7cm for the case of this design. The HE11 modes have field distributions that are azimuthally symmetric and are uniformly polarized. The axial symmetry of the field distribution provides an excellent coupling to the lowest Gauss-Laguerre beam mode (m=0). A maximum power coupling ratio $|c_o|^2$ of 98% of the fundamental mode of Gaussian beam and HE11 mode can be achieved if beam radius w is equal to 0.644a of, where a here is the diameter of the FH. Some of the design guidelines used in this paper have been well researched and well established in the literature, such as the coupling of Gaussian beam into the radiating elements is well covered in chapter 7 in [7].

The following sections will show the steps taken for the design of the on-axis Gaussian beam parameters for the 22 and 200 GHz bands. Once that is done the specifications for the FH are chosen, basic type of antenna choice is made with estimated losses associated with it. We used ray tracing with (Zemax) in order to optimize the spot size at focus.

A. 200 GHz Quasi-optics system

One of the 200 GHz science requirements is to meet a pointing accuracy between the two aircraft of 0.5°. Roughly speaking that forces the diameter of the lens antenna to be 15 cm. Since we are using a 30 cm diameter lens, the 200 GHz FH is used to illuminate the lens with very large edge taper producing a beam size roughly equivalent to uniformly illuminating a 15 cm lens. Using $G_{193.5G}=20\log(\pi D/\lambda)$ with D=15cm, and $G_{193.5G}$=49.66 dB, the 1-D HPBW is determined from (1) [8]:

$$G_{193.5G} \sim 30'000/(\phi_x.\phi_y) \quad (1)$$

$\phi_x=\phi_y=0.57^o$ for symmetrical antenna illumination.
The 1-D edge taper (T_e) defines the normalized E-field at the antenna with respect to its aperture radius [9].

$$T_e\,(\text{dB}) = [\phi\,(\text{in rad})/(\lambda/D)-1.02]/0.0135 \quad (2)$$

From equation (2), T_e is found to be 67 dB. From the T_e we determine all the parameters of the Gaussian beam propagation at the lens, and propagating the beam backward to the FH to determine the beam waist w_o. The beam radius at the antenna aperture is easily calculated also from [9].

$$\alpha = 0.115*T_e\,(\text{dB}) = (r_a/w_a)^2 \quad (3)$$

For 1-D, w_a= 5.4 cm**,** and selecting an initial distance from the FH to the back surface of the antenna to be $z_{193.5G}$=12.1"= 30.73 cm, we can solve for w_o, and then for z_0 using (4) and (5):

$$z_o = \pi w_o^2/\lambda_{193.5G} \quad (4)$$

$$w(z)^2 = w_o^2[1+(z/z_0)^2] \quad (5)$$

$$R_{193.5G}=Z_{193.5G}\,(1+(\pi w_{o\_193.5G}{}^2/(\lambda_{193.5G}Z_{193.5G})^2) \quad (6)$$

$$\theta_o \cong 1.18\frac{\lambda}{\pi\omega_o} \quad (7)$$

Where z=0 plane is defined to be z_o a distance away from the aperture of the FH.
z_o = confocal distance (Rayleigh length)=14.9 mm.
w_o= beam waist=2.701mm (where the E- field is at maximum) and the wave front is flat (or plane) and the on-axis phase shift ϕ_o is 0.
$R_{193.5G}$ =31.46 cm at the back surface of the lens (at z = $z_{193.5G}$= 30.734 cm away from the 200 GHz FH.
$\theta_o \cong 12.4^o$ is the far-field divergence angle.
In most quasi-optics system designs it is important to address the location of the phase center of the beam with respect to the FH aperture Δpc (offset of the phase center relative to the beam waist) [7]

$$\Delta pc = -\frac{(\pi\omega_o{}^2/\lambda)^2}{z} \quad (8)$$

$$z = \frac{R_h}{1+[\lambda R_h/\pi(0.644a)^2]^2} \quad (9)$$

R_h is the slant length of the FH. Δ_{pc} becomes more important if higher modes of the Gaussian beams are included in the design. The calculated value for Δ_{pc} was ~ 1.11 cm.

Typically the E-field that excites the waveguide feeding into the FH is linearly polarized, however in order to minimize the losses due to the relative orientation between the 2 aircrafts while in the air, we chose to have a circular polarizer to be placed between the waveguide and the FH, the output then is RHC (Right Hand Circular) for one of the instrument and LHC (Left Hand Circular) on the other one. Adding the polarizer makes the total length of the assembly to be 6.06 cm, which causes the 22 GHz band FH to be placed at least 6.06 cm behind the 200 GHz FH. Since the transmitted and the received power through the 22 GHz system are considerably higher than those of the 200 GHz system, it was important to make sure that the lens antenna was designed to have maximum gain and minimum losses at the 200 GHz center band. Consequently, the 22 GHz signal will see more losses, both due to the FH blockage and due to the defocusing of the lens. However as mentioned earlier, these losses can be mitigated by increasing the transmitter power.

The output beam waist (w_{out}) and the distance from the system output plane to the output beam waist are calculated using Gaussian beam transformation method. Since $z_{in}=f=30.73cm$ (the beam waist is located at the front focal plane), $z_{out}=f$ (output beam waist (image waist) is found to be at the back focal plane of the lens with w_{out}=5.37 cm. This is very different from the imaging in geometric optics, since we expect placing a source at the front focal plane would produce and image at infinity. The Gaussian beam will behave much more like a spherical wave if z_o/z approaches 0, or $z>>z_o$. As a result the output divergence angle is found to be close to 0.5°, and the output beam is for the most part is collimated. Also $z_{o\_200Gout}$=5.89 m with system magnification at maximum M_{max}=20.

B. 22 GHz Quasi-optics system

As a first step, in the evaluation of 22 GHz quasi–optic system design, we used CST microwave to simulate a simplified version of the system. Here, we were interested in examining the quality of the 22 GHz beam pattern in the far-field region when the spider and the 200 GHz FH obscuration are placed 6.06 cm in front of the 22 GHz feed. In order to simplify and shorten the simulation, a smooth walled FH model was used rather than corrugated horn such as the one that is used in the actual system. The spider was added (without the 200 GHz FH), Microwave absorbers [MODEL ECCOSORB MFS-124] will be added in the real system to minimize reflections inside the 22 GHz beam path in particular, and reduce unwanted reflections in general. The dimensions of the 22 GHz FH were estimated for 22.5 GHz excitation. Figure (3) shows the simplified geometry used without including the 183 GHz FH.

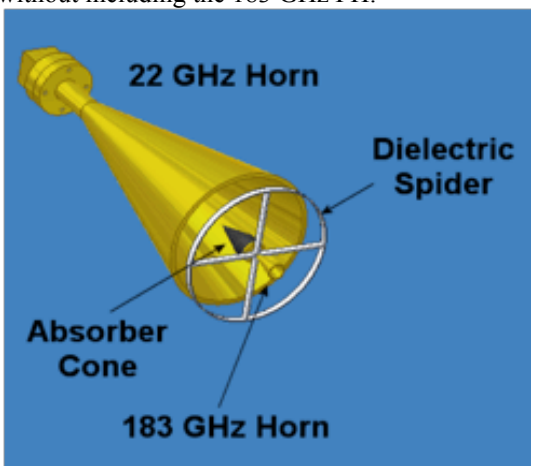

Figure 3: The simplified quasi-optics system diagram showing both the 22GHz & 200 GHz FHs, 30 cm lens antenna, a dielectric spider and absorber cone.

Figure (4) shows the 22 GHz FH E and H-plane beam patterns, at the spider legs and 45° away from spider legs. The dotted and solid lines represent the orthogonal polarization patterns (E & H-planes). While the 22 GHz beam pattern is degraded by the presence of the spider and the central blockage, the overall system performance is still very good, thanks to the amount of transmitted power at 22 GHz (~100 mW per tone). The Gaussian beam propagation calculation for the 200 GHz system was repeated here for the 22 GHz with a few differences. Assuming 0.55 aperture efficiency, the gain of the circular lens antenna at the middle of the 22 GHz band is 34 dB using (10).

$$G \approx 10 \log [0.55(\pi D/\lambda)^2] \quad (10)$$

Using, the same Gaussian propagation equations for one dimension we find that for the 22 GHz beam, $\phi_x=\phi_y=3.304^o$, T_e= 20.5 dB, w_a= 9.99 cm at the antenna back surface. At z_{22G}=36.79 cm (30.73+6.06cm) away from the lens, $w_{o\text{-}22G}$ =1.58 cm, $z_{o\text{-}22G}$= 5.9 cm, and the radius of curvature at the back surface of the lens is R_{22GHz} =36.92 cm, $\theta_o \cong 18.2^o$.

C. Lens selection and Zemax simulation

The distance between the 2 aircrafts is very large (from 20 km to 1000 Km). With this configuration modeled as having a point source at a vey large distance such that received waves behave like plane waves ($R_{in}\sim\infty$). We use a single lens to focus the incoming beam to a smallest spot possible at the 200 GHz FH aperture. Using the thin lens equation below:

$$1/R_{out\_200GHz} = 1/R_{in\_200GHz} + 1/f_{200GHz} \quad (11)$$

$R_{out\_200G}=f_{200G}$=30.79 cm. Since we are interested in a simple, low-cost design, low absorption loss, therefore the smallest central thickness is desired. However, at the same time the material of the lens needs to be hard, mechanically stable, relatively inexpensive for higher altitude environment, cheap and easy to machine. At first two materials were considered, Rexolite (n=1.59 @ 200 GHz), and HDPE [8] (n=1.529). Rexolite was found to have high losses (close to 4.8 dB for a center thickness t_c =6.5 cm), therefore HDPE (High Density Polyethylene) was chosen as the basis of the lens design. The estimated absorption losses of < 1 dB for the same t_c. At first our model used values of index of refraction found in the literature [10]. We were then able to use empirical values based on an in-house index of refraction measurement of samples of the actual material the lens was fabricated from. Using Time Domain Spectroscopy (TDS) techniques for 30 samples the average measured n at 193.5GHz was=1.520 with maximum sample-to-sample measuring error of 0.092%.

The empirically obtained index of refraction was used to improve the Zemax lens design parameters. Spherical-plano shaped lenses were avoided for this application as they tend to be thicker (t_c=10.85 cm) compared to hyperbolic-plano lens designs. In a first step we optimized the lens design for the 200 GHz beam only without including the 22.5 GHz beam. The optimization criteria chosen were: First, to achieve the smallest focused spot size, and second, to achieve the lowest optical path difference (OPD) with respect to the chief ray in the y direction (the x- directions results are identical), all this while keeping the thickness as small as possible, and therefore minimizing transmission loss. . The optimized spot size, and the OPD are shown in figure (5) top and bottom, respectively. Previously, the estimated aperture diameter of the 200 GHz FH was 11.36 mm.

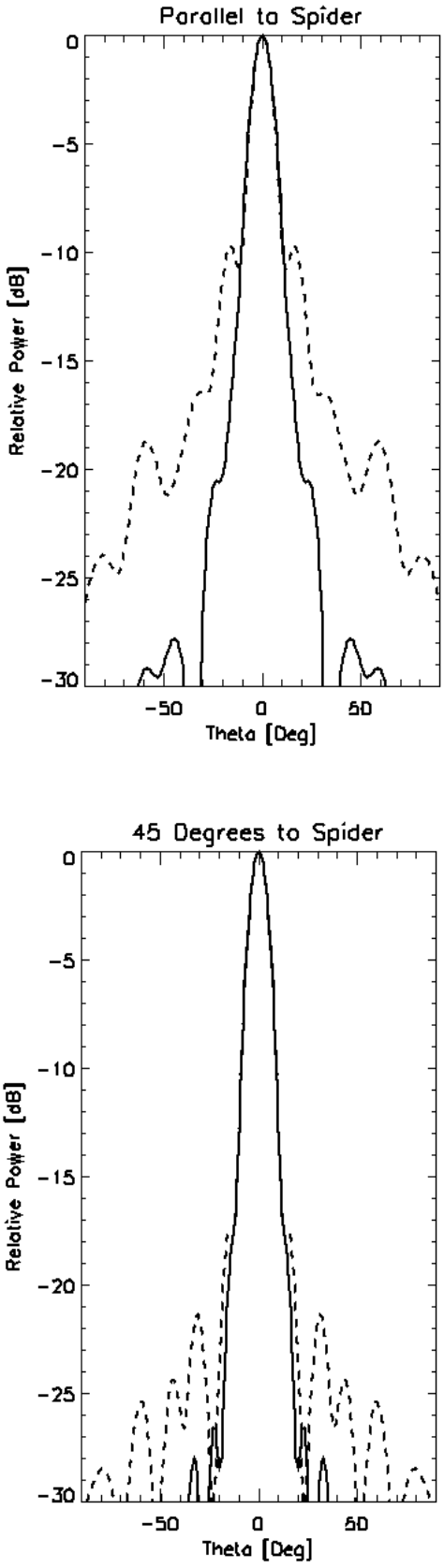

Figure 4: E & H-field beam pattern (solid and dotted line respectively), with respect to the angle θ, with θ=0 (top) (parallel to the dielectric spider), and 45° tilt away from it (bottom).

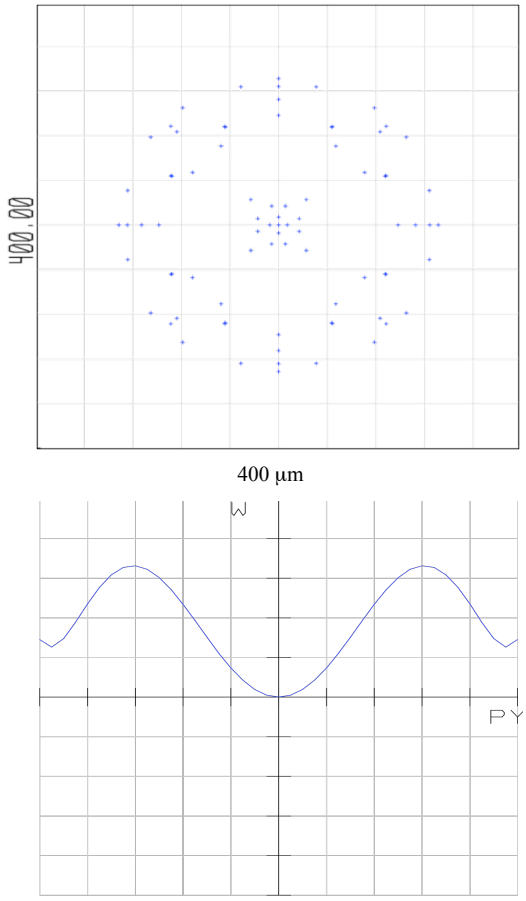

Figure 5**:** The spot size in in μm at the 200 GHz FH aperture (top), 40 μm/div and the optical path difference (bottom) with respect to chief ray in waves at the wavelength of 0.155 cm.

The design and manufacturing of the FHs were done by Quinstar microwave after providing them with required Gaussian beam paramteres. A spot size of ~260μm is well centered within the 10.58 mm diameter of the FH. The optimum value of the central thickness of the lens was 7.5 cm. The first Zemax optimization for the 200 GHz beam caused the incoming 22 GHz beam to be focused at ~ 5.3 cm to the right of the 22 GHz FH aperture, which caused the 22 GHz system to operate in a defocused mode. The antenna gain reduction due to the defocus can easily be calculated using (12) in [9].

$$\varepsilon_a(\delta) = \frac{\varepsilon_a(0)}{1 + (\delta / z_o)} \tag{12}$$

Where $\varepsilon_a(\delta)$ is the antenna efficiency for a Gaussian illuminated beam with a defocusing distance of δ=5.3cm, and $\varepsilon_a(0)$ is the antenna efficiency when the Gaussian beam is in focus. The defocusing losses becomes 10 log $(\varepsilon_a(\delta)/\varepsilon_a(0))$ which results to about 2.3 dB gain reduction. As mentioned earlier, the losses in the 22.5 GHz system are easily compensated by the provided extra gain provided through various attenuators placed in the 200 GHz microwave chain. The resulting defocused beam radius centered at the edge of the 22 GHz FH is obtained to be w_{22Gnew}= 2.24 cm, indicating

a growth of only 6.5 mm from its $w_{o\ 22G}$ location. After a sequence of design optimization in Zemax, the resulting lens surface produced fits exactly polynomial of the 10th degree.

III. Loss Calculation & measurments

Since the goal of this design is to balance the performance of the 200 GHz system with that of the 22 GHz system, we designed and produced an AR-layer in the two lens surfaces to reduce reflections of the 200 GHz transmitted and received beams. Our approach has well been established and has been used for many years in radio astronomy [11]. The method involves machining circular grooves in the two surfaces such that the resulting surfaces acts like a matching layer with an effective index of refraction n_{eff}, such that $n_{eff} \sim n^{1/2}$. This procedure provides better matching impedance to free space resulting in a reduction of reflection loss. For frequencies up to 400 GHz, grooving the surfaces with circular grooves is done via micro machining with a CNC milling. This method creates a well-defined topologies with depth $d=\lambda/4n^{1/2}$ depth and pitch values, and a filling factor that determines the value of the n_{eff}. In [12] and [13] 1-D structures have been investigated and used in the past such as rectangular, multi-step, or sine wave-grooves, and 2-D structures are also known with structures like rectangles and holes. 1-D structures are more likely to be polarization dependent and might be birefringent than 2-D structures. The design selections for the groove's specific pitch, depth and filling factor were done by studying examples in the listed literature as well as by using the program "SCATTER " written by R. Padman [14]. Reflection losses for a single surface dielectric material can be expressed for normal incident as in (13):

$$L_{Ref}(dB) = 10\log\left(\frac{(n-1)^2}{(n+1)^2}\right) \qquad (13)$$

Calculating L_{Ref} show that for n=1.52, $L_{Ref\_ungrooved}$ =-13.7 dB, however for a grooved surface with estimated $n_{eff}= n^{1/2}$=1.23, $L_{Ref\_grooved}$= -19.7 dB. The above calculation ignores the effect of variation of index of refraction with frequency, which will have small impact on the calculated reflection. The effect of the second surface reflectance is also small compared to the material loss for a center thickness of d=7.6 cm. In order to count for the 2nd surface reflection, we reduced and suitably parameterized eq (59) in [15] for normal incident in air media ($n_1=n_3=1$), which resulted in $L_{Ref\_2surf\_ungrooved} \cong$-14 dB, and $L_{Ref\_2surf\_grooved}$ = -19.75 dB. From the reported values of loss tangent tan(δ) for dielectric materials, its found to be ≅ 4e-4 for HDPE. The resulting material attenuation loss for a 7.6 cm thick is found to be -0.85 dB at 183 GHz and -0.94 dB at 203 GHz, which is much larger than the extra loss added due to the 2nd surface reflection. The result of the averaged through transmission and material loss of simulating two grooved surfaces sandwiching the lens material using program "SCATTER " with thickness of 6.4 cm is shown in Figure (6).

The total transmission T_{total}, where $T_{total} = T_{surface1or2}^2 + A$ (the material loss =-0.85 dB) is found to be -0.92 dB at 183 GHz. Therefore $T_{surface1or2}$ is found to be 0.992. The reflection of a single grooved surface based on R=1-T is then ≅ -20.9 dB. Repeating the same calculations for f=203 GHz results in a single surface reflection -19.34 dB. The simulation and the earlier calculations above are in a very good agreement showing approximately an average reduction in reflection of about ≅ 6 dB. The concentric lines of grooves were applied to the center of the two surfaces of the lens up to r=15 cm, since the main lobe of the 200 GHz beam will be centered on that area. Comparative reflection measurement was performed using a THz Time Domain Spectroscopy (THz-TDS) system. In THz-TDS ultra short pulses are generated that last only a few picoseconds. Each pulse creates broadband radiation from 0.05 to 2 THz. At the receiver the E-field of the terahertz pulse is sampled and digitized. A delayed femtosecond optical pulse gates the receiving dipole antenna "ON" through an identical LT-GaAs semiconductor. By repeating this procedure and varying the delay of the gating laser pulse, it is possible to scan the THz pulse and construct its E-field as a function of time with 0.1picosecond resolution over a 1 nanosecond time period. Subsequently, a Fourier transform is used to extract the frequency spectrum from the time-domain data. THz TDS was used to measure the reflection of the grooved lens surfaces as shown in Figure (7).

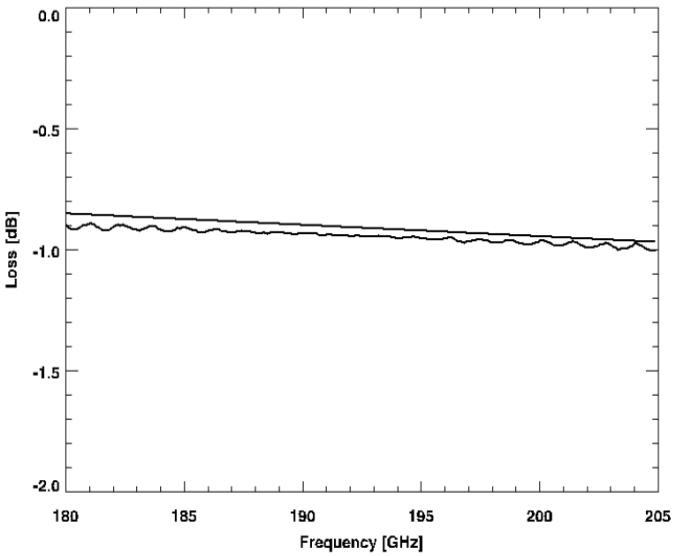

Figure 6: Reflection and absorption losses versus frequency for a grooved HDPE lens with n=1.52. The straight line is just the material losses, and the Fabry-Perot reflection line is material losses plus reflection losses, simulated using program "SCATTER " written by R. Padman [13].

The linearly polarized in the x-direction THz E-field beam is propagated through the Polarization Beam Splitter (PBS), and a Quarter Wave Plate (QWP) that changes the Polarization from linear to circular. As the beam reflects back from the lens surface, the incident circularly polarized beam changes its handedness. By the time it pass through the QWP in the second pass, it become linearly polarized in the same plane as the wires of the PBS such that it reflects into the THz Rx. In this experiment the QWP used was centered at ≅ 350 GHz, which will make the polarization more elliptical rather than linear, which could introduce some coupling and or cross polarization losses into the receiver. The results of the reflection measurements are shown in Figure (8). The red curve represents the reflection coefficient of the grooved surface and the blue for the un-grooved surface. Since the

majority of the incident beam will be transmitted through the lens in the case of grooved and the un-grooved surfaces, the measurement of the reflected beam in this case is clearly dominated by the 1st surface reflection (-13.7 dB) since adding the material and 2nd surface reflection will give (-13.6 dB). At 183 GHz we see a difference of ≅ 8 dB and 9 dB at 203 GHz between the grooved and un-grooved data plots, which is 2 to 3 dB higher than what was predicted in the simulation and calculations. Understanding fully the reasons of the differences between the calculated and measured values for both the grooved and un-grooved surfaces are not totally resolved nor concluded in this paper, and will continue to be a topic of an on going study in our group. However, it is our understanding that the factors that contribute to these differences could range anywhere between losses due to beam alignment errors, beam proper coupling, cross polarization and stigmatism losses. For example, it is highly likely that difference of ≅ 4.3 dB observed between the calculated and the measured reflection in the un-grooved surface case could be related to the rise of polarization losses at the receiver. Since the QWP used is not centered at 200 GHz it will result in producing an elliptically polarized beam incident on the surface of the lens, which could cause polarization losses at the receiver after passing through the rest of system.

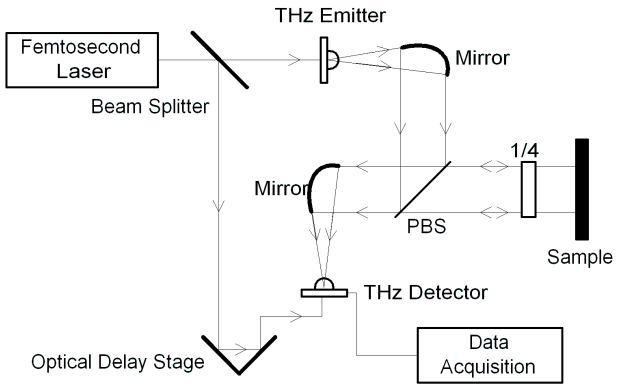

Figure 7: THz Pulse TDS reflection measurments setup diagram of the grooved and un-grooved surfaces of the HDPE lens.

Another example will be the observed difference of ≅6 to 7.2 dB between the calculated and measured values of reflection in the case of the grooved surface could be due to the cross polarization losses and stigmatism. The latter loss factors might be present when a polarized wave is incident on a material with effectively an anisotropic surface. This situation is highly likely to occur since the index of refraction of the grooved surface exhibits a variation in the x-and y-directions due to the grooves, which that might not be symmetric. Cross polarization and stigmatism losses produced could both be in the order of 0.2% of the reflected beam which calculated to be ≅ (-7.8 dB), as has been shown in J. Lamb analysis and simulation work in [16]. A much more comprehensive analysis for these previously discussed topics may be carried

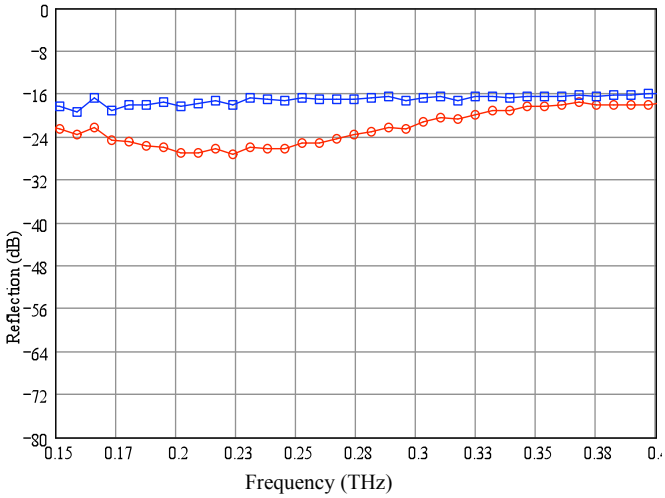

Figure 8: THz TDS reflected E-field measurements for the grooved (red) lens flat surface and un-grooved (blue) flat surface with respect to frequency (THz). Reflected losses for the un-grooved surface at both 183 GHz and 203 GHz is ≅ -18 dB, while at the grooved surface the total losses are -26 dB at 183 GHz and -27.2 dB at 203 GHz.

out in future publications. It is important to also mention that the design for a large bandwidth AR dielectric coating and optimized for selective frequencies using the grooving technique is extremely hard to make especially as the frequency of interest increases. Our initial design specifications for the groove's depth such that the grooves will induce the maximum matching to air in the middle of the 200 GHz band ≅ 193.5 GHz. The resulting desired groove depth was found to be 0.314 mm, however the measured grooves depth in the delivered HDPE lens that is under test was 0.264 mm exceeding the tolerance of ±0.025mm. The difference between the preselected and measured depths caused a shift of ≅ 36.5 GHz in the minimum observed reflection from the grooved surface as shown in Figure 8, where at 230 GHz the reflection is at minimum of -28 dB. However, from the overall quasi-optics system design point of view, a minimum of a 6 dB reduction in the reflection across the desired 200 GHz band has been met, and is considered very acceptable.

IV. FUTURE WORK

From the quasi-optics modeling and design point of view, it will be very useful to remodel in much more details the 200 GHz FH and spider assembly to look at its effect on the blockage of the 22 GHz far-field pattern using CTS. Also with the help of Zemax, a suite of simulations of the system tolerance will be very helpful in order to determine the impact of any mechanical deviations and environmental variations to the optics performance. From the testing point of view, it will be very useful to measure the phase center of the two beams, so that final optimization of the beam coupling is possible. System end-to-end far field lab bench optics measurement is needed to characterize the performance of the entire link. This will be followed by a comprehensive instrument-to-instrument test with the instruments transmitting from roof top to roof top between two high building across the university campus After

final adjustment on all fronts of the system, ATOMMS will be ready to be tested in a radio occultation configuration with the systems installed in the gimbal sections of the two NASA WB57-F aircrafts as explained in the introduction to this work.

V. Conclusion

This paper describes the ATOMMS instrument quasi-optical system design and provides some of the preliminary testing made so far. The design of the ATOMMS instrument can be found in another paper in this volume [5]. Once fully built and tested, the ATOMMS instrument promises to revolutionize the way of doing atmospheric science measurement and will add increased accuracy, resolution and coverage in the sounding of the Earth's atmosphere. An important aspect not covered in this work is the relevance of atmospheric turbulence in the propagation of microwaves through the atmosphere. This in fact is an error source that ATOMMS researchers have been investigating with dedication [17]. We have also covered the procedure used in designing both the 22 GHz and the 200 GHz TX/RX optics system by means of employing Gaussian beam propagation, and geometric optics. The goal was to make the coupling of the 200 GHz & the 22 GHz beams into their perspective feed horns as high as possible, and to minimize both reflections back to the transmit FHs and losses. This paper included the reflection measurements, and the effect of anti-reflection coating the surface of the lens by adding concentric grooves, which resulted in a reduction in the reflection of 6 dB. As we have mentioned before, considerable work is still needed to verify the performance of the lens, understanding further the extra losses seen in the measurement.

Acknowledgements

I am very thankful to all the people who at any level have helped and added so much in their very special talented way into the making of the 1st one of a kind ATOMMS instrument. ATOMMS is supported by the NSF Major Research Instrumentation Program under award # ATM-0723239.

References

[1] Cicerone, Ralph J., et al., *Climate Change Science: An Analysis of Some Key Questions* National Research Council, 2001, National Academy Press, pp 23-24

[2] http://www.atmo.arizona.edu/personalpages/kursinsk/papers/ATOMMS_051605_corrected.pdf.

[3] E. R. Kursinski, E. R., et al., "The Active temperature, ozone and moisture microwave spectrometer (ATOMMS)", in ECMWF/EUMETSAT GRAS SAF Workshop Proceedings, The pplications of GPS Radio Occultation Measurements. S. Healy Ed. 2008.

[4] http://www.nasa.gov/returntoflight/launch/wb57_chasejets.html.

[5] C. Groppi, E. R. Kursinski, D. Ward, Angel Otarola, Kate Sammler, Michael Schein, S. Al Banna, B. Wheelwright, S. Bell, W. Bertiger, M. Miller, H. Pickett "ATOMMS: the Active Temperature, Ozone and Moisture Microwave Spectrometer" Proceedings of the International Symposium on Space Terahertz Technology, in press, 2009.

[6] G. Fjeldbo, A. J. Kliore, and V. R. Eshleman (1971), 'The neutral atmosphere of Venus studied with the Mariner V radio occultation experiments", *The Astronomical Journal*, 76(2), 123-140.

[7] P. F. Goldsmith, *QuasiOptics Systems,* NewYork, IEEE Press, John Wiley & Sons, 1998 pp157-176.

[8] Constantine A. Balanis, *Antenna Theory: Analysis and Design*, New York, NY, John Wiley & Sons,1997, 2nd Edition, p60.

[9] P. F. Goldsmith, *QuasiOptics Systems,* NewYork, NY, IEEE Press, John Wiley & Sons, 1998 pp129-139.

[10] A. Sengupta, A. Bandyopadhyay, B.F. Bowden, J.A. Harrington and J.F. Federici, Characterization of Olefin copolymers using terahertz spectroscopy" The Institution of Engineering and Technology 2006, 13October2006. Electronics Letters online no: 20063148 1

[11] G. A. Ediss & T. GlobusÜ, "60 to 450 GHz Transmission and Reflection Measurements of Grooved and Un-grooved HDPE Plates", ALMA Memo No. 347, National Radio Astronomy Observatory Charlottesville, VA 22903 ÜDept of EE, University of Virginia.

[12] D. Raguin, G. Morris, "Analysis of anti-reflection-structured surfaces with continuous one-dimensional surface profiles", Applied Optics 32 (14) (1993) 2581–2598.

[13] D. Raguin, G. Morris, Anti-reflection structured surfaces for the infrared spectral region, Applied Optics 32 (7) (1993)

[14] Nancyjane Bailey and A. R. Kerr, Electronics Division Technical Note No. 155 PROGRAM "SCATTER" FOR THE ANALYSIS OF DIELECTRIC MATCHING LAYERS, 12 September 1989. http://www.gb.nrao.edu/electronics/edtn/edtn155.pdf

[15] Born and Wolf, *Principles of Optics,* London, UK, 4th edition1970, PERGAMON PRESS S.A.R.L, P61

[16] J.Lamb, "Cross-Polarization and Astigmatism in Mathcing grooves." International Journal of Infrared and Millimeter Waves Vol.17, No. 12, 1996.

[17] Otarola, A.C., The effects of turbulence in an absorbing atmosphere on the propagation of microwave signals used in an active sounding system. Ph.D. dissertation, The University of Arizona, United States -- Arizona. ProQuest Digital Dissertations @ University of Arizona database. (Publication No. AAT 3336701) 2008.